

Melting of Aluminum Cluster Cations with 31–48 Atoms: Experiment and Theory[†]

Colleen M. Neal,[‡] Anne K. Starace,[‡] Martin F. Jarrold,^{*,‡} Kavita Joshi,[§]
Sailaja Krishnamurty,[§] and Dilip G. Kanhere^{*,§}

Chemistry Department, Indiana University, 800 East Kirkwood Avenue, Bloomington, Indiana 47405 USA and
Department of Physics and Centre for Modeling and Simulation, University of Pune, Ganeshkhind,
Pune-411 007, India

Received: February 3, 2007; In Final Form: June 14, 2007

Heat capacities have been measured as a function of temperature for aluminum clusters with 31–48 atoms, complimenting previous measurements for larger clusters. Peaks in the heat capacities (due to the latent heat) indicate melting transitions. Large size-dependent fluctuations in the melting temperatures are found in the 31–48 atom size regime, with the lowest melting temperature differing from the highest by close to 400 K. There are also large variations in the latent heats; some clusters show prominent peaks in their heat capacities, whereas for others the peak is virtually absent. A first effort is made to explain the main features of these results by investigating the geometries of the clusters using first principles density functional methods. It appears that clusters that show strong first-order phase transitions have geometries with more uniform bonding (i.e., more similar bond energies and bond lengths) than clusters that lack a strong first-order phase transition. The variation in the melting temperature is associated with the core–surface connectivity and the average coordination of the atoms in the cluster.

Introduction

What happens to the melting transition as the size of an object is reduced into the nanometer regime has been a topic of interest for many years. It has only recently become possible to measure the melting transitions of metal clusters as a function of the number of atoms they contain. The first studies were performed on sodium clusters.^{1–5} Measurements have now been performed on gallium,^{6–8} sodium chloride,⁹ tin,^{10,11} and aluminum clusters.^{12,13} These latter studies have focused on clusters in the 10–10² atom size range. Information on the melting transitions has been obtained from heat capacity measurements^{1–13} and ion mobility measurements.^{8,10} In the former, the signature of melting is a peak in the heat capacity resulting from the latent heat. The center of the peak is usually taken as the melting temperature, whereas the area under the peak provides a measure of the latent heat. In the mobility measurements, an abrupt change in the mobility due to a change in the shape or volume of the cluster is taken to indicate melting (the mobility of a gas-phase ion depends on its average collision cross section with the buffer gas, which in turn depends on the shape and volume).^{14,15} Ideally one would like to use both measurements to investigate the melting transitions, but so far this has only been done in the case of gallium clusters where inflections or jumps in the mobilities were found to be correlated with peaks in the heat capacities. In cases where the heat capacities do not show a peak, a signature of melting was still evident in the mobilities, suggesting that some clusters melt without a significant latent heat. In addition to the large variations in the latent heats, there are also large variations in the melting

temperatures. For example, the melting temperature varies by more than 300 K for gallium cluster cations with 30–50 atoms.⁷

The substantial fluctuations in both the melting temperatures and the latent heats found in the experimental studies have provided the motivation for a number of theoretical studies directed at understanding these results.^{16–24} The cause of the size-dependent fluctuations in the melting temperatures, in particular, has received a lot of attention. The origin of the fluctuations is complex because the melting temperature of a cluster depends on both the enthalpy and the entropy changes associated with the melting transition. The entropy and enthalpy changes determined experimentally are correlated,^{4,7,13} making the fluctuations in the melting temperatures even more abstruse. Small particles are expected to have melting temperatures that are lower than the bulk material because of their higher surface to volume ratio. Depressed melting temperatures have been observed for several systems in the cluster size regime, for example, Na_n⁺, (NaCl)_nNa⁺, and Al_n⁺. In some cases, for example, Ga_n⁺ and Sn_n⁺, the clusters have elevated melting temperatures. The melting temperature elevation has been attributed to the clusters having different geometries and, more importantly, different bonding than the bulk (i.e., the clusters are not bulk fragments).

In this manuscript we report heat capacity measurements for aluminum cluster cations with 31–48 atoms. These studies compliment previous experimental studies of larger aluminum clusters.^{12,13} In addition to the experimental studies, we report calculations for aluminum clusters containing 31, 34, 37, 39, 40, 44, and 46 atoms. These clusters were chosen to represent the variations in the melting behavior observed in the 31–48 atom size regime. With decreasing cluster size, one expects that fluctuations in the melting temperature and the latent heat will become larger, and indeed this is observed. Adding or subtracting a single atom often causes an abrupt change in the melting behavior. The previous experimental work on the melting of

[†] Part of the special issue “Richard E. Smalley Memorial Issue”.

* To whom correspondence should be addressed. E-mail: M.F.J.: mfj@indiana.edu; D.G.K.: kanhere@unipune.ernet.in.

[‡] Indiana University.

[§] University of Pune.

aluminum clusters has inspired several theoretical studies.^{20–22} Noya, Doye, and Calvo used Gupta and glue potentials to investigate the melting of clusters with 49–62 atoms.²⁰ These potentials favor icosahedral and polytetrahedral structures, respectively. Heat capacity curves calculated using the glue potential were featureless for most cluster sizes. On the other hand, the heat capacities derived using the Gupta potential showed a well-defined peak for most cluster sizes, indicating a first-order-like transition. However, the results did not match the observed size dependence of the melting transitions. This was interpreted as indicating that the clusters do not have icosahedral or polytetrahedral geometries. Zhang, Zhang, and Zhu used a Gupta potential to investigate the melting of aluminum clusters containing 55, 56, and 57 atoms.²¹ They studied the melting of a number of different structural isomers with the goal of explaining dips observed in the heat capacities of Al_{56}^+ and Al_{57}^+ (the dips, which precede the peaks due to melting, have been attributed to annealing transitions from less stable structural isomers¹²). Aguado and Lopez used density functional theory (DFT) to investigate the structures and stabilities of Al_n^+ with $n = 46–62$.²² The lowest energy structures found in these studies were fragments of the bulk face-centered cubic (fcc) lattice with stacking faults and a strong preference for (111) faces. A significant change in the shape was found at Al_{55}^+ and Al_{56}^+ (from a shape that is roughly a square pyramid to one that is roughly octahedral). This shape change could be responsible for the abrupt change in the melting temperature that occurs at this point.

Experimental Methods

The heat capacities reported here were measured using multicollision-induced dissociation. A detailed description of the method has been provided elsewhere,¹³ so only a brief overview is provided here. The method is based on determining the shift in the dissociation threshold as a function of the temperature of the clusters. As the temperature is raised, the internal energy increases, and there is a corresponding decrease in the energy that must be added to reach the dissociation threshold. Initially, the internal energy of the solid-like clusters increases gradually, but there should be a sharp increase in the internal energy, due to the latent heat, when the cluster melts. The jump in the internal energy, or the corresponding spike in the heat capacity, is a signature of melting.

Singly-charged aluminum cluster cations are generated by laser ablation of a liquid aluminum target in a flowing helium buffer gas. Use of a liquid metal target provides signals that are more stable than those obtained with solid targets, which must be rotated and translated to prevent the laser from making a pit in the target.²⁵ After formation, the clusters are carried into a temperature variable extension where their temperature is set through collisions with the helium buffer gas. After the clusters are thermalized they exit the source and are accelerated and focused into a quadrupole mass spectrometer, which is set to transmit a particular cluster size. The mass selected cluster ions are subsequently focused into a collision cell containing 1 Torr of helium gas. As the ions enter the collision cell, collisions with the helium convert the cluster ions' kinetic energy into internal energy and kinetic energy of the helium collision partners. If the ions' initial kinetic energy is high enough, the clusters are heated to the point where they dissociate. Ultimately, the ions' kinetic energy is thermalized, and then they travel across the collision cell under the influence of a weak electric field. Some of the ions exit the collision cell through a small aperture and are focused into a second quadrupole mass

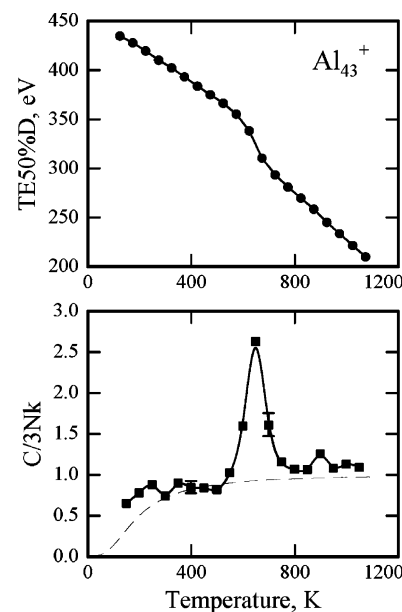


Figure 1. Plot of TE50%D against temperature (top) and a plot of the heat capacities derived from the derivative of TE50%D with temperature (bottom). The heat capacities are plotted in terms of the classical value $3Nk$ where $3N = 3n - 6 + 3/2$, n is the number of atoms in the cluster, and k is the Boltzmann constant. The thin dashed line in the lower plot shows heat capacities calculated with a modified Debye model that accounts for the finite size of the cluster. Error bars show typical uncertainties (\pm one standard deviation).

spectrometer, where they are mass analyzed. Ions that are transmitted through the second quadrupole are detected by a collision dynode and dual microchannel plates.

Experimental Results

Mass spectra are recorded as a function of the cluster ions' translational energy as they enter the collision cell, and the translational energy required for 50% of the ions to dissociate (TE50%D) is determined from a linear regression. TE50%D is measured as a function of the temperature of the extension. The plot of TE50%D against temperature obtained for Al_{43}^+ is shown in the top panel of Figure 1. The relatively sharp drop in the TE50%D values at approximately 650 K is attributed to the latent heat associated with a melting transition. The derivative of TE50%D with respect to temperature is proportional to the heat capacity. The proportionality constant is the fraction of the cluster ions' kinetic energy that is converted into internal energy in a collision between the cluster and a helium atom. This quantity is determined from an empirically corrected impulsive collision model.^{26–28} For the clusters studied here the fraction is about 5%. This fraction is small because helium is a poor collision partner, and it was selected as the collision gas for this reason. In the method employed here, changes in the collision-induced activation of the ions compensate for changes in the internal energy due to the temperature. With a poor collision gas, a large change in the cluster ions' kinetic energy is required to compensate for small changes in the internal energy. This amplification is a critical feature of the method.

The bottom panel of Figure 1 shows heat capacities derived from the TE50%D values shown in the top panel. The heat capacities are plotted in terms of the classical value $3Nk$, where $3N = 3n - 6 + 3/2$, n is the number of atoms in the cluster, and k is the Boltzmann constant. The thin dashed line in the bottom panel of Figure 1 shows heat capacities calculated with a modified Debye model that accounts for the finite size of the

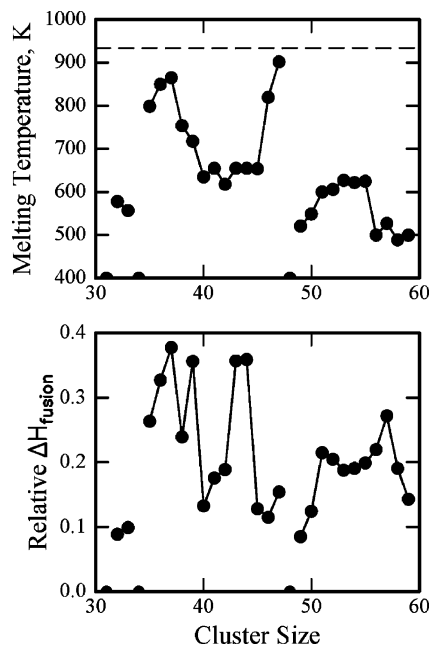


Figure 2. Plots of the melting temperatures and latent heats against cluster size for clusters with 31–59 atoms. The horizontal dashed line in the upper plot shows the melting point of bulk aluminum (934 K). Clusters with 31, 34, and 48 atoms do not have a significant peak in their heat capacities within the temperature range examined.

cluster.²⁹ The peak in the heat capacities at about 650 K indicates the melting transition. The peak in the heat capacity is over 200 K wide. Macroscopic crystalline objects have a single well-defined melting point. The broad melting transition found here is a consequence of the small size of the cluster. We take the center of the peak to be the melting temperature. This may not be the temperature where the free energy of the liquid-like cluster is the same as for the solid-like. The area under the peak is the latent heat associated with the melting transition. The area is obtained from a numerical integration where we assume a linear interpolation between the heat capacities of the liquid and solid clusters. Plots of the melting temperatures and latent heats for aluminum cluster cations with 31–59 atoms are shown in Figure 2. The results for clusters with 49–59 atoms were taken from our previous studies and are reproduced here to show the variations over a larger cluster size range. The latent heats are plotted relative to the bulk value on a per atom basis. Three clusters in the 31–59 atom size range (31, 34, and 48) lack a significant peak in their heat capacities (see below), and for these clusters the melting temperatures and latent heats are not available.

The dashed line in the upper half of Figure 2 shows the melting temperature of bulk aluminum (934 K). The measured melting temperatures all lie below the bulk melting point, but there are enormous fluctuations in the melting temperatures for clusters with 31–48 atoms. Peaks in the melting temperatures occur at 36–37 atoms and 46–47 atoms. The peak maxima (~900 K) are close to the bulk melting point. Between the maxima, the band of clusters with 40–45 atoms all have melting temperatures around 650 K. The clusters with the lowest melting temperatures in the plot are those with 56–59 atoms, these clusters have melting temperatures around 500 K. Thus the melting temperatures shown in Figure 2 vary, by about 400 K, with the number of atoms in the cluster. The latent heats (the bottom panel of Figure 2) also show large variations with cluster size.

Heat capacity plots are shown in Figure 3 for a representative selection of clusters (Al_{31}^+ , Al_{34}^+ , Al_{37}^+ , Al_{39}^+ , Al_{40}^+ , Al_{44}^+ ,

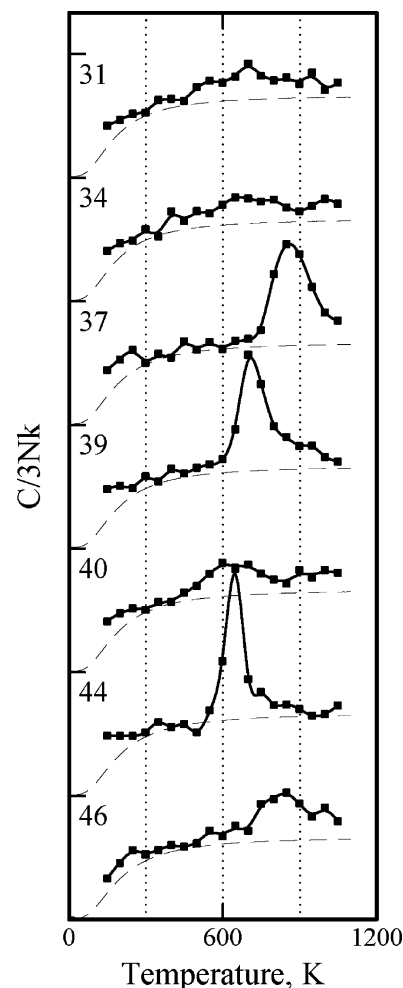


Figure 3. Heat capacities recorded for aluminum cluster cations with 31, 34, 37, 39, 40, 44, and 46 atoms.

and Al_{46}^+). Some clusters, such as Al_{31}^+ and Al_{34}^+ , do not show a significant peak in their heat capacities. The absence of a peak may indicate that the melting transition occurs outside the temperature range examined in the experiments or that melting occurs without a significant latent heat. Clusters with 35–39 atoms have relatively large latent heats. These clusters also have high melting temperatures. There is a drop in the latent heats for clusters with 40–42 atoms, and then there is a sudden jump at 43 and 44 atoms. There is no corresponding increase in the melting temperatures for Al_{43}^+ and Al_{44}^+ : the melting temperatures remain flat, whereas the latent heats show a sharp maximum. There is clearly no correlation between the latent heats and the melting temperatures.

Computational Details

As a first attempt to understand the experimental results present here, calculations were performed to identify the ground states for critical cluster sizes. The calculations were done on neutral clusters, whereas the measurements were performed on cations. However, the charge is not expected to make a substantial difference to the results for clusters in the size regime examined here. Approximately 300 geometries were optimized for each of the clusters under consideration. The initial configurations were obtained either from a constant-temperature molecular dynamic simulation performed at four different temperatures between 600 and 1000 K or derived from favorable geometries for other cluster sizes. The configurations generated through the above approaches were optimized using the first

principles density functional method.^{30,31} We used Vanderbilt's ultra soft pseudo potentials³² within the local density approximation (GGA) for describing the core–valence interactions. An energy cutoff of about 9.50 Ry is used for the plane wave expansion of the wave function with a convergence in the total energy on the order of 0.0001 eV.

Once the ground state geometries are obtained, various structural and electronic properties are calculated. Specifically, we analyze the shape of the cluster, the eigenvalue spectrum, the coordination numbers, the distribution of the shortest bonds, and the total charge density. We have also calculated the distribution of atoms from the center of mass of the cluster and the shape deformation parameter, ϵ_{def} . The shape deformation parameter is defined as eq 1;

$$\epsilon_{\text{def}} = \frac{2Q_x}{Q_y + Q_z} \quad (1)$$

where $Q_x \geq Q_y \geq Q_z$ are the eigenvalues, in descending order, of the quadrupole tensor (eq 2).

$$Q_{ij} = \sum_I R_{iI} R_{jI} \quad (2)$$

Here, i and j run from 1 to 3, I runs over the number of atoms, and R_{iI} is the i th coordinate of atom I relative to the center of mass of the cluster. $\epsilon_{\text{def}} = 1$ (i.e., $Q_x = Q_y = Q_z$) indicates that the cluster has the same distribution in all three directions. Larger values of ϵ_{def} indicate that the cluster's shape deviates from spherical.

Simulation Results and Discussion

We have investigated the ground state geometries of clusters with 31, 34, 37, 39, 40, 44, and 46 atoms and analyzed the differences in their structure and bonding. These cluster sizes were chosen to reflect the changing nature of the heat capacities in the size regime examined in the experiments. The clusters considered here can be classified into two main groups, one having a well-defined melting transition, as seen for Al_{37} , Al_{39} , and Al_{44} , and the other with almost a continuous transition, as observed in Al_{31} and Al_{34} . Some clusters (i.e., Al_{40} and Al_{46}) fall between these extremes and exhibit a weak melting peak. There are two interesting features present in the measured heat capacities the first is the variation in the size and shape of the peak, and the other is the substantial change (almost 400 K) in the melting temperature as a function of cluster size. Here, we investigate the possibility of a correlation between these features and the nature of the ground state geometry of the cluster as revealed through the geometric features as well as through the nature of the electronic bonding. Hence, we begin our discussion by analyzing the trends in the evolution of the geometry along the series examined.

In Figure 4 we show the lowest energy geometries found for Al_{31} , Al_{34} , Al_{37} , Al_{39} , Al_{40} , Al_{44} , and Al_{46} in our geometry search. For the purpose of visualization, two atoms are connected by a bond if the distance between them is less than 2.8 Å (the bulk bond distance is 2.82 Å). It can be seen from Figure 4 that these medium-sized aluminum clusters do not show any clear rotational symmetry. Similarly deformed structures have been found for aluminum clusters by Akola et al.,³³ although they investigated different sizes than those studied here. The variation in the shape of the clusters is shown through the deformation parameter ϵ_{def} (see eqs 1 and 2), which is plotted in Figure 5. The value of ϵ_{def} for Al_{37} , Al_{44} , and Al_{46} is nearly one, indicating that these clusters have similar distributions along all three

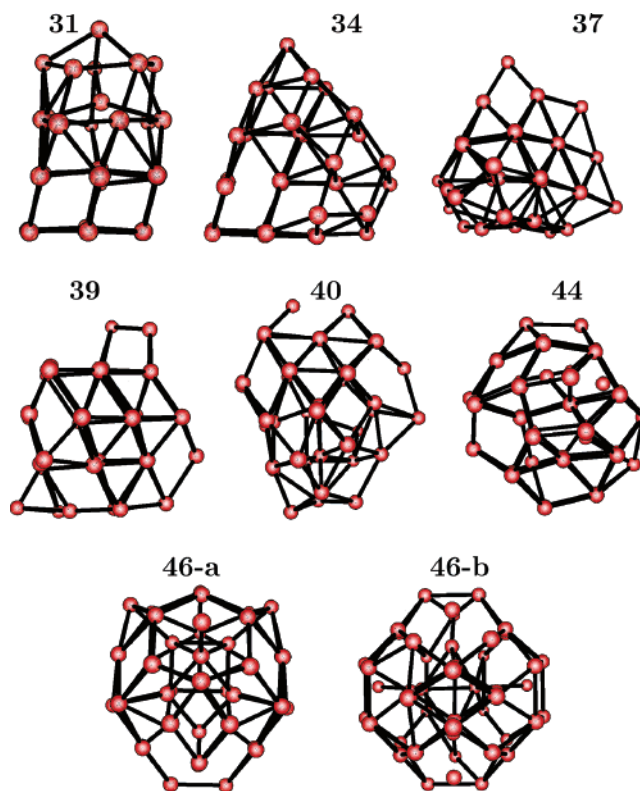


Figure 4. The lowest energy structures found for aluminum clusters with 31, 34, 37, 39, 40, 44, and 46 atoms. Two nearly degenerate geometries are shown for Al_{46} . Two atoms are connected by a bond if the distance between them is less than 2.8 Å.

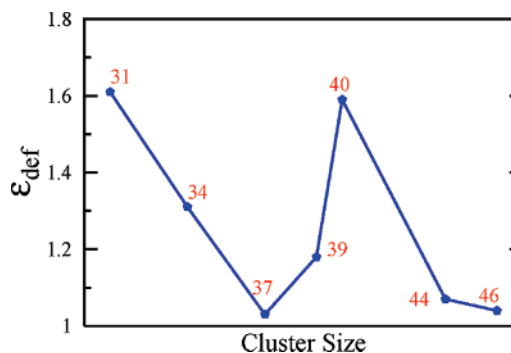


Figure 5. Deformation parameter (see eqs 1 and 2) as a function of cluster size. Al_{37} , Al_{44} , and Al_{46} have ϵ_{def} values close to 1.0, indicating that they have nearly the same distributions along all three orthogonal axes.

orthogonal axes. A closer look at the geometries in Figure 4 reveals that the geometries of Al_{31} , Al_{34} , and Al_{40} are more open, as seen by the presence of voids and atoms with low connectivity. We have also calculated average distances between planes of atoms, and for Al_{31} , Al_{34} , and Al_{40} it is on the order of 3.0 Å, as compared to the other clusters where it is on the order of 2.81 Å or less. It turns out that addition of three atoms to Al_{34} leads to compact and well connected planes for Al_{37} , with the shortest interplanar bond distances of 2.73 Å. The structure remains compact and well connected up to Al_{39} . Addition of one more atom to Al_{39} results in an open and nonspherical Al_{40} cluster, with a sudden increase in ϵ_{def} from 1.18 to 1.59 (see Figure 5). The geometry of Al_{44} is nearly spherical. Al_{46} has two nearly degenerate ground states, both of which are compact and spherical. Interestingly, two geometries were found for this cluster in previous ion mobility measurements,³⁴ whereas isomers were not found in these experiments for any of the other

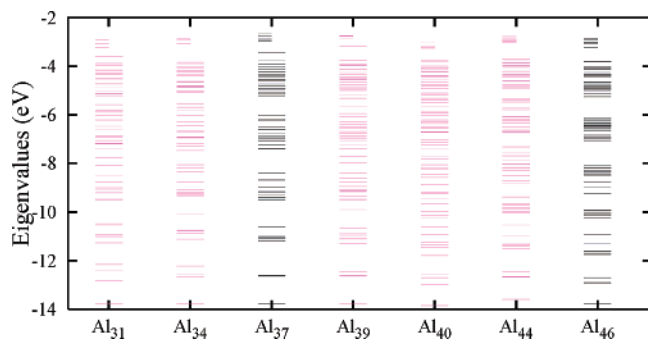


Figure 6. Eigenvalue spectra for the ground-state geometries of aluminum clusters. Note that the eigenvalue spectra for Al₃₇ and Al₄₆ are bunched together. Both of these clusters have high melting temperatures (above 800 K).

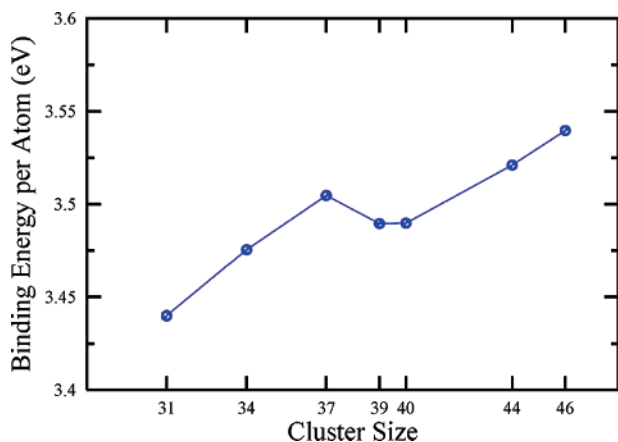


Figure 7. Binding energy per atom as a function of size of the cluster. The binding energy per atom for Al₃₇ and Al₄₆ are large relative to their neighbors.

clusters for which calculations were performed here. It may be noted that the structures that are compact and nearly spherical (with ϵ_{def} values of ≈ 1) have a well-defined melting peak in the heat capacity curve, whereas open structures such as Al₃₁, Al₃₄, and Al₄₀ (with a higher ϵ_{def} value) have a broad heat capacity curve showing an almost continuous transformation. Some of these evolutionary trends are also reflected in the eigenvalue spectra, which are shown in Figure 6. The spectra of Al₃₇ and Al₄₆ show distinct gaps with bunching of eigenvalues, whereas those of Al₃₁, Al₃₄, and Al₄₀ show a relatively even spread of eigenvalues, indicative of more disorder. The grouping of the levels seen for 37 and 46 is due to the near-spherical shape of these clusters (see Figure 5). These clusters adopt near-spherical shapes because they are at or near electronic shell closings.³⁵ It may be recalled that Al₃₇ and Al₄₆ have a relatively high melting temperature of approximately 850 K. At this point it is worth examining the variation in the binding energy for these clusters. In Figure 7 we show the binding energy per atom as a function of cluster size. The binding energy per atom for Al₃₇ is a local maximum.

As already mentioned above, there are two key features observed in the experiments: (1) the variation in the size and shape of the peaks in the heat capacities, and (2) the variation in the melting temperatures. First, we focus on the variation in the size and shape of the peaks in the heat capacity. In the experiments, it has been observed that Al₃₄ has a continuous solid-like to liquid-like transition, whereas Al₄₄ exhibits the narrowest peak in the series; hence, it will be beneficial to focus on these two clusters to understand the cause of such dramatically different finite temperature behaviors. Our earlier studies

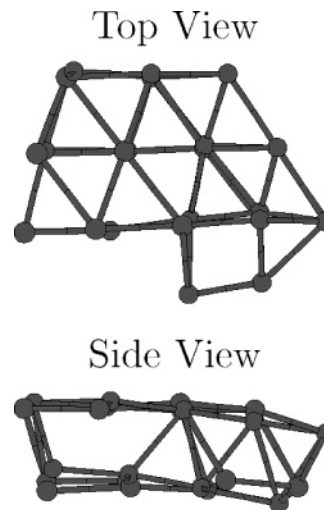


Figure 8. A fragment of Al₃₄ is shown to illustrate the void formation. The top view shows the absence of defects on the surface. The side view shows voids between the two surfaces.

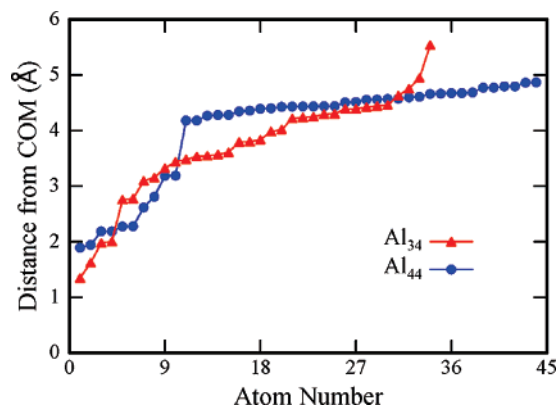


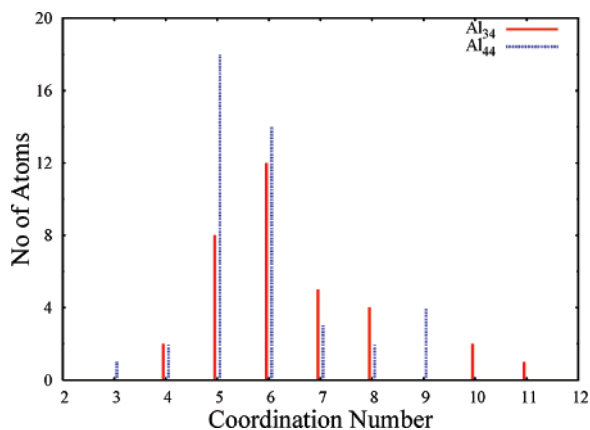
Figure 9. Distribution of atoms from the center of mass (COM) for Al₃₄ and Al₄₄. Formation of an outer shell is evident for Al₄₄ whereas Al₃₄ shows an almost continuous distribution of atoms around the COM.

of gallium clusters¹⁹ have demonstrated that the ground-state geometry of a cluster affects its finite temperature behavior significantly. Ga₃₀ with a “disordered” ground state leads to an almost continuous solid-like to liquid-like transition, whereas Ga₃₁ with an “ordered” ground state exhibits a well-defined peak in the heat capacity curve. We understand the meaning of “order” here as follows: an ordered structure has most of the atoms experiencing a similar environment or, in other words, most of the atoms are bonded with similar strength so that their response to the increase in the temperature will be similar. As has been already pointed out, the ground state of Al₃₄ is much more disordered than that of Al₄₄ and contains internal voids. The ground state of Al₃₄ can be thought of as being formed by several almost parallel planes of atoms connected to each other through intraplaner bonds that are stronger than the interplaner ones. The strained interfaces that give rise to the missing bonds and voids in this cluster are illustrated in Figure 8. This figure shows a fragment of the Al₃₄ cluster selected to illustrate void formation. In contrast, the ground state of Al₄₄ is more spherical. Because of the reconstruction of the surface of this cluster, there are hardly any voids or defects. Another interesting observation is the presence of a well-defined geometric shell structure for atoms in the case of Al₄₄. In Figure 9 we show the distribution of atoms from the center of mass for Al₃₄ and Al₄₄. The x -axis shows the atom number and the y -axis indicates its distance from the center of mass. A substantial difference between the

TABLE 1: Coordination Numbers for the Atoms in the Lowest Energy Geometries Found in the Calculations for Aluminum Clusters^a

coordination number	cluster size						
	31	34	37	39	40	44	46
4	3	2	4	6	3	3	3
5	6	8	4	5	10	18	10
6	10	12	7	4	9	14	17
7	5	5	13	13	7	3	12
8	3	4	6	4	6	2	3
9	3	0	0	2	3	4	1
10	1	2	2	2	2	0	0
11	0	1	1	3	0	0	0
average	6.39	6.41	6.70	6.85	6.50	5.89	6.11

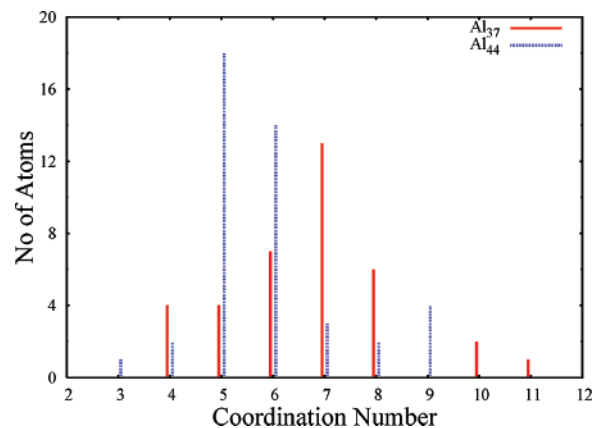
^a The first column indicates the coordination number and successive entries indicate the number of atoms with that coordination number for each cluster size.

**Figure 10.** Number of atoms as a function of coordination number for Al₃₄ and Al₄₄. For Al₄₄, 32 out of 44 atoms have either 5- or 6-fold coordination.

distributions for Al₃₄ and Al₄₄ is evident. Al₄₄ has a well defined outer shell consisting of 34 atoms that are almost equidistant from the center of mass of the cluster. In contrast, Al₃₄ has a more continuous distribution of atoms.

Another indicator for order in a cluster comes from the coordination numbers (i.e., the number of nearest neighbors for each atom). In Table 1 we show the coordination numbers for all the atoms in the clusters studied. The first column in the table indicates the coordination number, and successive entries indicate the number of atoms with that coordination number for each cluster size. The average coordination numbers range from 5.89 to 6.70. There does not appear to be a strong relationship between the size of the peaks in the heat capacity and the coordination numbers. To understand the origin of the differences in the heat capacity plots it is necessary to also consider the connectivity of the atoms and the geometries. In Figure 10 we show the coordination numbers for Al₃₄ and Al₄₄. For Al₄₄, most of the atoms (32 out of 44) have either 5- or 6-fold coordination. Thus, 73% of the atoms have almost the same coordination. Furthermore, all of these atoms are part of the surface (one shell) and are connected to each other. In the case of Al₃₄, the largest group with the same coordination is 12 atoms with 6-fold coordination. However, these atoms are not connected but are spread-out all over the cluster.

All these observations indicate that Al₃₄ is a more disordered structure than Al₄₄, in the sense discussed above. When such a disordered system is heated, the response of the individual atoms will be different for different atoms or group of atoms, leading to a near continuous heat capacity curve. Another important

**Figure 11.** Number of atoms as a function of coordination number for Al₃₇ and Al₄₄. For Al₃₇, 80% of the atoms have 6-fold or higher coordination, in contrast to Al₄₄, which has about 57% of the atoms (i.e., 25 out of 44) with a coordination number of 6 or more.

point is that the characterization of order in a finite-size system is subtle, and a single indicator like the coordination number is inadequate. A deeper analysis involving connectivity and the formation of islands of atoms with similar bonding is required.

We now present an analysis of the geometries of Al₃₇ and Al₄₄, both of which show well-defined peaks in their heat capacities, but their melting temperatures differ by about 250 K. In both of these clusters the atoms can be classified as either core atoms, which are completely embedded inside the cluster, or surface atoms. In the case of Al₃₇ the average distance between the core atoms and surface atoms is 2.92 Å, as compared to the core–surface distance of 3.3 Å seen in Al₄₄. Another significant difference appears in the coordination number shown for these clusters, which are compared in Figure 11. The average coordination of core atoms for Al₃₇ is 9.7, whereas for Al₄₄ its 7.8. Thus, the surface atoms are more strongly bound to the core atoms in Al₃₇ than in Al₄₄. Furthermore, for Al₃₇ about 29 atoms out of 37 (~80%) have a coordination number of 6 or more, whereas in case of Al₄₄ the number of atoms with a coordination number of 6 or more is much less (i.e., 25 atoms out of 44 [~57%]). We believe that the combination of the stronger core–surface interaction and the larger number of atoms with higher coordination numbers is responsible for the higher melting temperature of Al₃₇ as compared to Al₄₄. A similar analysis for another cluster that shows a high melting temperature, namely, Al₄₆, is consistent with this observation. Our understanding in this regard is also consistent with the results of Aguado and Lopez²² for sodium clusters, where they found a strong correlation between variation in the melting temperature and core–surface distances. We have also observed similar behavior for gallium clusters with 30–55 atoms.³⁶

Conclusions

The melting temperatures of small particles are expected to be lower than that of the bulk material because of the increase in the surface-to-volume ratio. A systematic decrease in the melting temperature is expected with decreasing particle size. In the small-size regime, the variations in the melting temperatures are no longer monotonic, and the size-dependent variations reported here are the largest found to date. In addition to the large size-dependent variations in the melting temperatures evident in Figure 2, the general trend appears to be one of increasing melting temperature with decreasing cluster size: the reverse from what is expected on the basis of the surface-to-

volume ratio. By analyzing the nature of the ground state we have been able to correlate the geometric features with the nature of the heat capacity curve. It is found that clusters whose geometries are open and show defects have a rather broad heat capacity curve. The high melting temperatures are associated with the existence of a strong core–surface interaction.

Acknowledgment. We gratefully acknowledge the support of the National Science Foundation (USA). We acknowledge C-DAC (PUNE) for providing us with supercomputing facilities. K.J. and D.G.K. thank the Indo-French Center for Promotion of Advanced Research (IFCPAR)/Centre Franco-Indien pour la Promotion de La Recherche Avancée (CEFIPRA) (project No. 3104-2) for partial financial support.

References and Notes

- Schmidt, M.; Kusche, R.; Kronmüller, W.; von Issendorff, B.; Haberland, H. *Phys. Rev. Lett.* **1997**, *79*, 99–102.
- Schmidt, M.; Kusche, R.; von Issendorff, B.; Haberland, H. *Nature* **1998**, *393*, 238–240.
- Schmidt, M.; Haberland, H. *C. R. Phys.* **2002**, *3*, 327–340.
- Schmidt, M.; Donges, J.; Hippler, Th.; Haberland, H. *Phys. Rev. Lett.* **2003**, *90*, 103401.
- Haberland, H.; Hippler, T.; Donges, J.; Kostko, O.; Schmidt, M.; von Issendorff, B. *Phys. Rev. Lett.* **2005**, *94*, 035701.
- Breaux, G. A.; Benirschke, R. C.; Sugai, T.; Kinnear, B. S.; Jarrold, M. F. *Phys. Rev. Lett.* **2003**, *91*, 215508.
- Breaux, G. A.; Hillman, D. A.; Neal, C. M.; Benirschke, R. C.; Jarrold, M. F. *J. Am. Chem. Soc.* **2004**, *126*, 8628–8629.
- Breaux, G. A.; Cao, B.; Jarrold, M. F. *J. Phys. Chem. B* **2005**, *109*, 16575–16578.
- Breaux, G. A.; Benirschke, R. C.; Jarrold, M. F. *J. Chem. Phys.* **2004**, *121*, 6502–6507.
- Shvartsburg, A. A.; Jarrold, M. F. *Phys. Rev. Lett.* **2000**, *85*, 2530–2532.
- Breaux, G. A.; Neal, C. M.; Cao, B.; Jarrold, M. F. *Phys. Rev. B* **2005**, *71*, 073410.
- Breaux, G. A.; Neal, C. M.; Cao, B.; Jarrold, M. F. *Phys. Rev. Lett.* **2005**, *94*, 173401.
- Neal, C. M.; Starace, A. K.; Jarrold, M. F. *J. Am. Soc. Mass Spectrom.* **2007**, *18*, 74–81.
- Clemmer, D. E.; Jarrold, M. F. *J. Mass Spectrom.* **1997**, *32*, 577–592.
- Wytttenbach, T.; Bowers, M. T. *Top. Curr. Chem.* **2003**, *225*, 207–232.
- Chacko, S.; Joshi, K.; Kanhere, D. G.; Blundell, S. A. *Phys. Rev. Lett.* **2004**, *92*, 135506.
- Manninen, K.; Rytönen, A.; Manninen, M. *Eur. Phys. J. D* **2004**, *29*, 39–47.
- Krishnamurty, S.; Chacko, S.; Kanhere, D. G.; Breaux, G. A.; Neal, C. M.; Jarrold, M. F. *Phys. Rev. B* **2006**, *73*, 045406.
- Joshi, K.; Krishnamurty, S.; Kanhere, D. G. *Phys. Rev. Lett.* **2006**, *96*, 135703.
- Noya, E. G.; Doye, J. P. K.; Calvo, F. *Phys. Rev. B* **2006**, *73*, 125407.
- Zhang, W.; Zhang, F.; Zhu, Z. *Phys. Rev. B* **2006**, *74*, 033412.
- Aguado, A.; Lopez, J. M. *Phys. Rev. Lett.* **2005**, *94*, 233401.
- Aguado, A.; Lopez, J. M. *J. Phys. Chem. B* **2006**, *110*, 14020–14023.
- Aguado, A.; Lopez, J. M. *Phys. Rev. B* **2006**, *74*, 115403.
- Neal, C. M.; Breaux, G. A.; Cao, B.; Starace, A. K.; Jarrold, M. F. *Rev. Sci. Instrum.* **2007**, *78*, 075108.
- Jarrold, M. F.; Honea, E. C. *J. Phys. Chem.* **1991**, *95*, 9181–9185.
- Jarrold, M. F.; Honea, E. C. *J. Am. Chem. Soc.* **1992**, *114*, 459–464.
- Jarrold, M. F. *J. Phys. Chem.* **1995**, *99*, 11–21.
- Bohr, J. *Int. J. Quantum Chem.* **2001**, *84*, 249–252.
- Vienna Ab Initio Simulation Package*; Technische Universität Wien, 1999.
- Kresse, G.; Furthmüller, J. *Phys. Rev. B* **1996**, *54*, 11169–11186.
- Vanderbilt, D. *Phys. Rev. B* **1990**, *41*, 7892–7895.
- Akola, J.; Manninen, M.; Häkkinen, H.; Landman, U.; Li, X.; Wang, L.-S. *Phys. Rev. B* **2000**, *62*, 13216–13228.
- Jarrold, M. F.; Bower, J. E. *J. Chem. Phys.* **1993**, *98*, 2399–2407.
- Knight, W. D.; Clemminger, K.; De Heer, W. A.; Saunders, W. A.; Chou, M. Y.; Cohen, M. L. *Phys. Rev. Lett.* **1984**, *52*, 2141–2143.
- Krishnamurty, S.; Joshi, K.; Zorriassatein, S.; Kanhere, D. G. *J. Chem. Phys.* **2007**, *127*, 054308.